

Anomalous Magnetoresistance beyond the Jullière Model for Spin Selectivity in Chiral Molecules

Tian-Yi Zhang,[†] Yue Mao,[†] Peng-Yi Liu,[†] Ai-Min Guo,[‡] and Qing-Feng Sun^{*,†}

[†]*International Center for Quantum Materials, School of Physics, Peking University,
Beijing 100871, China*

[‡]*Hunan Key Laboratory for Super-microstructure and Ultrafast Process, School of Physics,
Central South University, Changsha 410083, China*

[¶]*Hefei National Laboratory, Hefei 230088, China*

E-mail: sunqf@pku.edu.cn

Abstract

The issue of anomalous high magnetoresistance, beyond the Jullière model, observed in nonmagnetic electrode-chiral molecular-ferromagnetic electrode devices has puzzled the community for a long time. Here, by considering the magnetic proximity effect which shifts the nonmagnetic-ferromagnetic interface toward chiral molecules, we show the anomalous high magnetoresistance beyond the spin polarization in ferromagnetic electrodes even in the very weak spin-orbit coupling. Our results are in excellent agreement with the experiments, demonstrating that the spin-orbit coupling plays a fundamental role in chiral-induced spin selectivity and the magnetic proximity effect can dramatically enhance the magnetoresistance. These results elucidate the interaction between chiral molecules and ferromagnetic electrodes and facilitate the design of chiral-based spintronic devices.

Chirality plays a fundamental role in nature and has attracted extensive interest among the chemistry, biology, and physics communities.^{1,2} In the last decade, a lot of work has studied the spin transport along chiral molecules,^{3,4} finding that spin-unpolarized electrons will become highly spin-polarized when transmitted through chiral molecules, namely the chiral-induced spin selectivity (CISS).⁵⁻⁷ This CISS holds great applications in spintronic devices. Historically, CISS was initially observed in stearyl lysine photoemission experiments in 1999.⁸ Since then, CISS has been reported in different chiral materials,⁹⁻¹¹ such as double-stranded DNA,^{3,12} α -helical proteins,¹³ and halide perovskites.¹⁴ To understand the physical mechanism behind CISS, many theories have been proposed.¹⁵⁻²⁶ The first kind of theory suggests that the helical structure and the spin-orbit coupling (SOC) of chiral molecules are key to generating large spin polarization for electrons passing through chiral molecules.¹⁵⁻¹⁷ In these works, the SOC strength is usually set to be about one-tenth of the inter-nucleobase or inter-amino acid hopping integral. The second kind of theory considers that CISS arises from the interaction between metal substrates with large SOC and chiral molecules.²¹ However, recent experiments demonstrate that CISS still exists in the absence of metal substrates, revealing substrates with large SOC are not necessary for CISS.²⁷⁻²⁹ Although many other models such as spin-dependent scattering,²² electron-phonon coupling,²³ and electron correlation²⁴ are proposed, the physical mechanism of CISS remains under debate.

In experiments, a variety of techniques have been employed to measure the CISS effect, including photoemission,³ electrochemistry,³⁰ fluorescence signals,³¹ and electrical transport,^{32,33} where the electrical transport method is extremely powerful for detecting the CISS effect. In electrical transport experiments, CISS is studied by measuring the magnetoresistance (MR) of a two-terminal nonmagnetic electrode-chiral molecule-ferromagnetic electrode (N-chiral molecule-FM) device,^{34,35} as shown in Figure 1a. When the magnetization direction of the FM electrode is oriented in positive or negative directions, the current flowing through the device differs, and one can obtain the MR and thus determine the spin selec-

tivity of chiral molecules.^{36,37} Provided that the spin-up and spin-down density of states (DOSs) in FM electrodes are ρ_{\uparrow}^{FM} and ρ_{\downarrow}^{FM} , respectively, the FM polarization is defined as³⁸ $P_{FM} = (\rho_{\uparrow}^{FM} - \rho_{\downarrow}^{FM})/(\rho_{\uparrow}^{FM} + \rho_{\downarrow}^{FM})$. Similarly, the spin polarization evaluating the CISS effect of chiral molecules is defined as $P_s = (n_{\uparrow}^{mol} - n_{\downarrow}^{mol})/(n_{\uparrow}^{mol} + n_{\downarrow}^{mol})$, where n_{\uparrow}^{mol} and n_{\downarrow}^{mol} are, respectively, the densities of spin-up and spin-down electrons passing through chiral molecules. According to the Jullière model,³⁹ the current I_{+M} under positive magnetization of FM electrodes is proportional to $n_{\uparrow}^{mol}\rho_{\uparrow}^{FM} + n_{\downarrow}^{mol}\rho_{\downarrow}^{FM}$. By reversing the magnetization, the spin-up and spin-down DOSs in FM electrodes exchange, and the current under negative magnetization satisfies $I_{-M} \propto n_{\uparrow}^{mol}\rho_{\downarrow}^{FM} + n_{\downarrow}^{mol}\rho_{\uparrow}^{FM}$. The experimentally measured MR can then be expressed as $MR = (I_{+M} - I_{-M})/(I_{+M} + I_{-M})$, which is equal to $P_s P_{FM}$. Accordingly, the MR is always smaller than the FM polarization P_{FM} as $|P_s| \leq 1$. FM electrodes used in experiments are usually composed of transition metals such as nickel (Ni), iron (Fe), and cobalt (Co), with P_{FM} about 33%, 44%, and 45%, respectively.⁴⁰ However, it has been widely reported that the MR associated with the CISS effect can reach 80%,^{41–43} which is much larger than P_{FM} . This violation of the Jullière model frequently appears in electrical transport experiments of the CISS and has been noticed for a long time.^{44–46} Many researchers find it incomprehensible and feel puzzled, but a satisfactory answer to this question remains elusive to this day.⁴⁷

In this Letter, we study the CISS in chiral molecules and demonstrate strong CISS even at extremely weak SOC regime. When the magnetic proximity effect (MPE) is introduced at the molecular end, an anomalous large MR far beyond FM polarization P_{FM} is found. We show that the MR is always lower than P_{FM} in the absence of MPE, and the MR completely disappears once either chirality or SOC vanishes, revealing their essential roles in the CISS and MPE is the origin of $MR > P_{FM}$. These findings well address the dilemmas mentioned above.

We first show the origin of the CISS effect in the nonmagnetic electrode-chiral molecule-nonmagnetic electrode (N-chiral molecule-N) device. The physical origin of CISS arises from

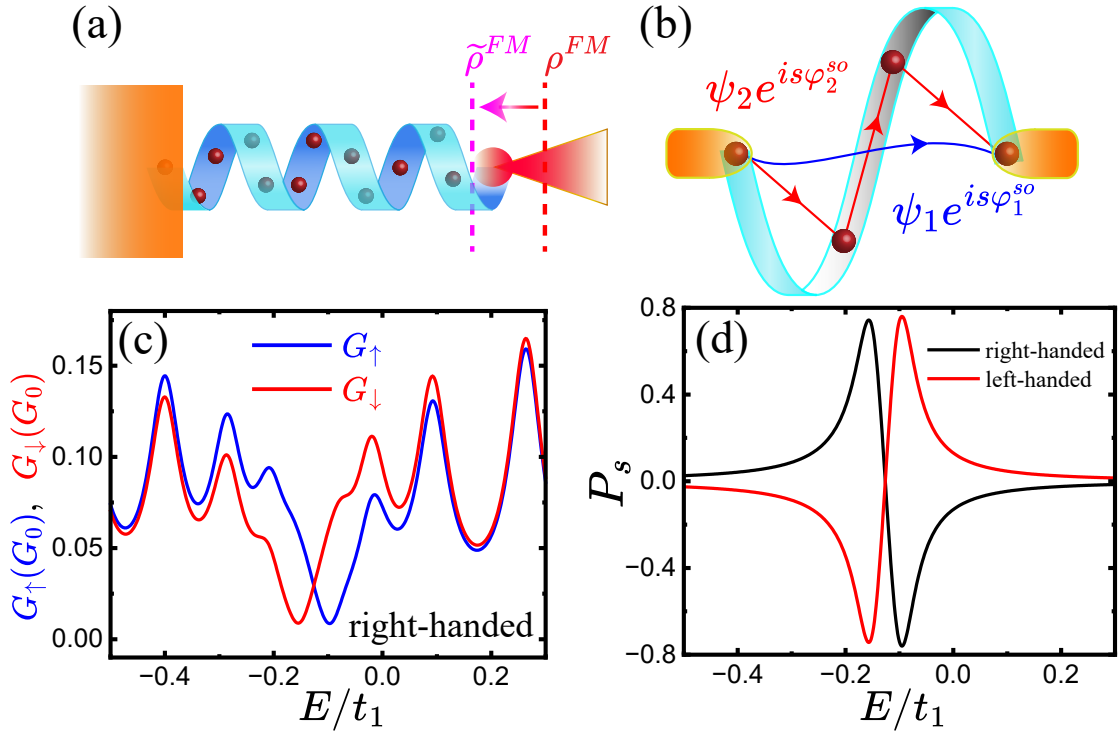


Figure 1: Schematic of chiral molecular model and the corresponding spin polarization. (a) Schematic of a N-chiral molecule-FM (or N) device. The right electrode is set to be nonmagnetic to study the spin polarization P_s for electron propagation through chiral molecules, or to be ferromagnetic to study the MR. In the presence of MPE induced by the FM electrode, the rightmost site of chiral molecules becomes magnetized. (b) Schematic diagram of two-pathway interference. (c) and (d) are conductances G_\uparrow , G_\downarrow and spin polarization P_s versus the energy E in N-chiral molecule-N device at extremely weak SOC $s_1 = 0.01t_1$. Here, E is the Fermi energy, t_1 is the intrachain hopping integral and $G_0 = e^2/h$ is the quantum conductance.

the multi-pathway helical structure and SOC of chiral molecules.^{15,16,48} There exist multiple pathways for electron propagation through chiral molecules, and the interference of electron wave-functions through these pathways is the basis for the CISS effect. If such interference is absent, CISS effect cannot occur in one-pathway molecules.¹⁵ Here, we consider the simplest case of two transport pathways as an example, as illustrated in Figure 1b, where ψ_1 and ψ_2 describe the wave-functions of electron propagation along pathway-1 and pathway-2, respectively, in the absence of SOC. Due to the chiral structure, the two pathways are usually different from each other with the phase difference being $\Delta\varphi_{12}$. In the presence of SOC, the two wave-functions are changed to $\psi_1 e^{is\varphi_1^{so}}$ and $\psi_2 e^{is\varphi_2^{so}}$, generating the spin-related phase factors.^{49,50} Here, $s = \uparrow (+)$ and $\downarrow (-)$ denote the up and down spin, respectively, and $\varphi_{1/2}^{so}$ are the phase related to the SOC. The total probability of electron propagation through the two pathways is proportional to $|\psi_1 e^{is\varphi_1^{so}} + \psi_2 e^{is\varphi_2^{so}}|^2 = |\psi_1|^2 + |\psi_2|^2 + 2|\psi_1||\psi_2|\cos(s\Delta\varphi_{so} + \Delta\varphi_{12})$ with $\Delta\varphi_{so} = \varphi_1^{so} - \varphi_2^{so}$, which depends on the electron spin. As a result, the CISS emerges. In realistic systems, there may be more than two interference pathways, and the magnitude of CISS effect is determined by the details of the molecule.

Let us study the spin transport properties of the N-chiral molecule-N device (see Figure 1a). We take the single-helical protein as an example,¹⁶ which can be described by a tight-binding Hamiltonian with SOC and multi-pathway structure:

$$\begin{aligned}
H_{cmolecule} = H_{mol} + H_{so} = & \sum_{n=1}^N \varepsilon_n c_n^\dagger c_n + \sum_{n=1}^{N-1} \sum_{j=1}^{N-n} [t_j c_n^\dagger c_{n+j} + h.c.] \\
& + \sum_{n=1}^{N-1} \sum_{j=1}^{N-n} [2is_j \cos(\varphi_{n,j}^-) c_n^\dagger \sigma_{nj} c_{n+j} + h.c.]
\end{aligned} \tag{1}$$

where $c_n^\dagger = (c_{n,\uparrow}^\dagger, c_{n,\downarrow}^\dagger)$ is the creation operator at site n , and the molecular length is N . ε_n is the on-site energy, t_j is the long-range hopping integral between sites n and $n+j$, and s_j is the corresponding SOC. σ_{nj} is a 2×2 matrix related to the molecular structure. $\varphi_{n,j}^- = j\Delta\varphi/2$, where $\Delta\varphi$ is the twist angle between two neighboring sites. The length of chiral molecule is

$N = 30$. The twist angle is set to $\Delta\varphi = 5\pi/9$ for right-handed molecules and $\Delta\varphi = -5\pi/9$ for left-handed molecules (see Section S1.1, S1.2, and Figure S1 in Supporting Information for the Hamiltonian, parameters, and multi-pathway structure). The robust explanatory power of this model is demonstrated by its successful explanation of key CISS-related phenomena, including the CISS effect in chiral molecules,¹⁷ the dynamic process of the CISS effect in electron donor–chiral molecule–acceptor systems,¹⁹ the spin polarization and magnetization effect in chiral molecules,²⁰ CISS-modulated spin-to-charge conversion,⁵¹ and inverse CISS effect.⁵² The structural parameters are identical to previous works,^{16,17} except that the SOC strength s_1 is set to be two orders of magnitude smaller than the intrachain hopping integral t_1 . Setting the hopping integral $t_1 = 100$ meV,⁵³ the SOC strength is only $s_1 = 1$ meV, which is consistent with the actual values in the experiments.^{6,9,54} Below we will show that this extremely weak SOC is sufficient to produce large spin polarization.

The conductance can be calculated using the Landauer-Büttiker formalism (see Section S1.3, S1.4 in the Supporting Information),⁵⁵ and the spin polarization is $P_s = (n_{\uparrow}^{mol} - n_{\downarrow}^{mol}) / (n_{\uparrow}^{mol} + n_{\downarrow}^{mol}) = (G_{\uparrow} - G_{\downarrow}) / (G_{\uparrow} + G_{\downarrow})$, where G_{\uparrow} and G_{\downarrow} correspond to the spin-up and spin-down conductances. Figure 1c shows G_{\uparrow} and G_{\downarrow} vs. Fermi energy E . One can see that G_{\uparrow} is different from G_{\downarrow} in a wide energy range. This indicates spin-unpolarized incident electrons from the left nonmagnetic electrode become highly spin-polarized when they transmit through chiral molecules to the right nonmagnetic electrode, a clear signature of CISS. Figure 1d shows the spin polarization P_s derived from Figure 1c. P_s can reach the value of 74.4% even at the extremely weak SOC with $s_1 = 0.01t_1$. The physical origin of CISS arises from the combination of SOC and multi-pathway interference, as shown in Figure 1b.

To demonstrate the significance of SOC and chirality, we calculate G_{\uparrow} , G_{\downarrow} , and P_s in the absence of either SOC or chirality and analyse the physical picture from the multi-pathway interference (see Section S1.5, Figures S2-S4, and Table S1 in the Supporting Information). In both cases, G_{\uparrow} and G_{\downarrow} completely overlap and P_s is exactly zero. Furthermore, P_s in

right-handed molecules are exactly opposite to that in left-handed molecules (see Figure 1d, Section S1.5 and Figure S2 in the Supporting Information). This indicates that chirality is the prerequisite for CISS, and the SOC plays a fundamental role in the CISS although it is extremely weak. Due to P_s of left-handed and right-handed molecules being exactly opposite, we present only the results for the right-handed molecules below.

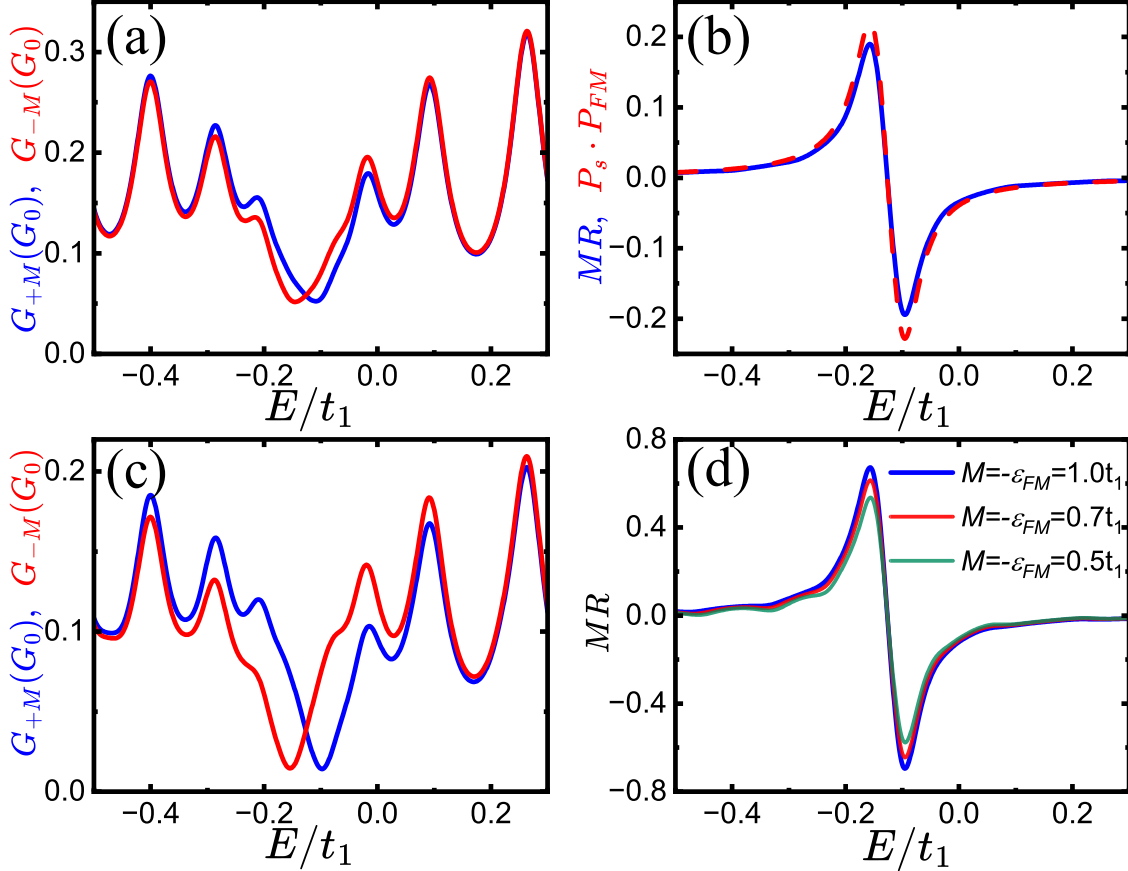


Figure 2: Conductance and MR in the N-molecule-FM device. (a) and (b) respectively show conductances G_{+M} , G_{-M} and MR, $P_s P_{FM}$ versus Fermi energy E in the device without MPE. Here $MR \leq P_s P_{FM} < P_{FM}$ implies the validity of the Jullière model. (c) Conductances G_{+M} and G_{-M} versus E by considering the MPE ($M = -\varepsilon_{FM} = t_1$). (d) MR in the presence of MPE for different MPE parameters, in which MR can be larger than $P_{FM} = 30\%$, implying the invalidity of the Jullière model. In (a-d), the SOC strength $s_1 = 0.01t_1$.

Next, we study the MR in N-chiral molecule-FM device, see Figure 1a. The FM polarization is fixed at $P_{FM} = 30\%$, a typical value of the FM tip/FM substrate used in the experiments. The MR is calculated by $MR = (G_{+M} - G_{-M}) / (G_{+M} + G_{-M})$, where $G_{+M}(G_{-M})$ represents the conductance for positive (negative) magnetization electrode (see

Section S1.3 in the Supporting Information). Figure 2a and Figure 2b display, respectively, the conductance and MR without MPE. The difference between conductances G_{+M} and G_{-M} is too small to yield a notable MR compared to the MR observed experimentally.^{36,37} In Figure 2b we also show the product of P_s and P_{FM} . MR is slightly smaller than $P_s P_{FM}$ only, which is consistent with the Jullière model. We emphasize that, for whatever the values of model parameters, $MR < P_{FM}$ always and the Jullière model holds. In the experiments, however, MR can be larger than P_{FM} and the Jullière model is violated.^{42,43}

To answer the question why $MR > P_{FM}$ in many experiments, we consider the MPE induced by the FM electrode. When two different materials are coupled together, their electronic wave-functions hybridize. Such hybridization becomes stronger at the end site of chiral molecules closest to the FM material because the discrete energy levels in the molecules are coupled to many states in the FM electrode. This MPE can be described by the Hamiltonian $H_{MPE} = \varepsilon_{FM} c_N^\dagger c_N + M c_N^\dagger \sigma_z c_N$, where M represents the magnitude of the magnetization, ε_{FM} represents the renormalization energy on the rightmost site (i.e. site N) closest to the FM electrode due to the MPE (see Sections S1.2 and S1.6 in the Supporting Information), and σ_z is the Pauli matrix for the z -direction. The values of M and ε_{FM} are about hundreds of meV.⁵⁶⁻⁵⁸ As illustrated in Figure 1a, the actual system consists of a nonmagnetic substrate, a chiral molecule with the rightmost site influenced by the MPE, and a FM tip. In the presence of MPE, the conductances and the MR can be calculated as before (see Section S1.3 in the Supporting Information). From Figure 2c, a large difference between G_{+M} and G_{-M} is shown, which is entirely different from Figure 2a without the MPE. Figure 2d displays the MR for different parameters of the MPE. It is clear that MR is dramatically enhanced and can achieve the value of 67.3%, greater than $P_{FM} = 30\%$. Moreover, with increasing the molecular length, MR also increases and can surpass 80% (see Figure S5a), which is in excellent agreement with the experiments.^{44,59} We also study the influence of dephasing and SOC⁶⁰⁻⁶⁴ on the MR, finding that high MR beyond P_{FM} is achieved in a large parameter range (see Figures S5b and S6 in the Supporting Information). To further

explore the influence of the MPE, in Figure 3a we calculate MR versus the parameters, M and ε_{FM} , related to the MPE, where the white-dashed line corresponds to the FM polarization $P_{FM} = 30\%$. One can see that MR can be greater than P_{FM} , indicating the violation of the Jullière model in a wide parameter range (red region in Figure 3a; note that these regions are accessible since M and ε_{FM} can attain values of hundreds of meV,^{56–58} i.e., a few t_1). To maintain this, M and ε_{FM} should have opposite sign, and the maximum of MR occurs for $M = -\varepsilon_{FM}$. On the other hand, when M and ε_{FM} have the same sign, MR is reversed and its absolute value exceeds P_{FM} as well (Figure 3a).

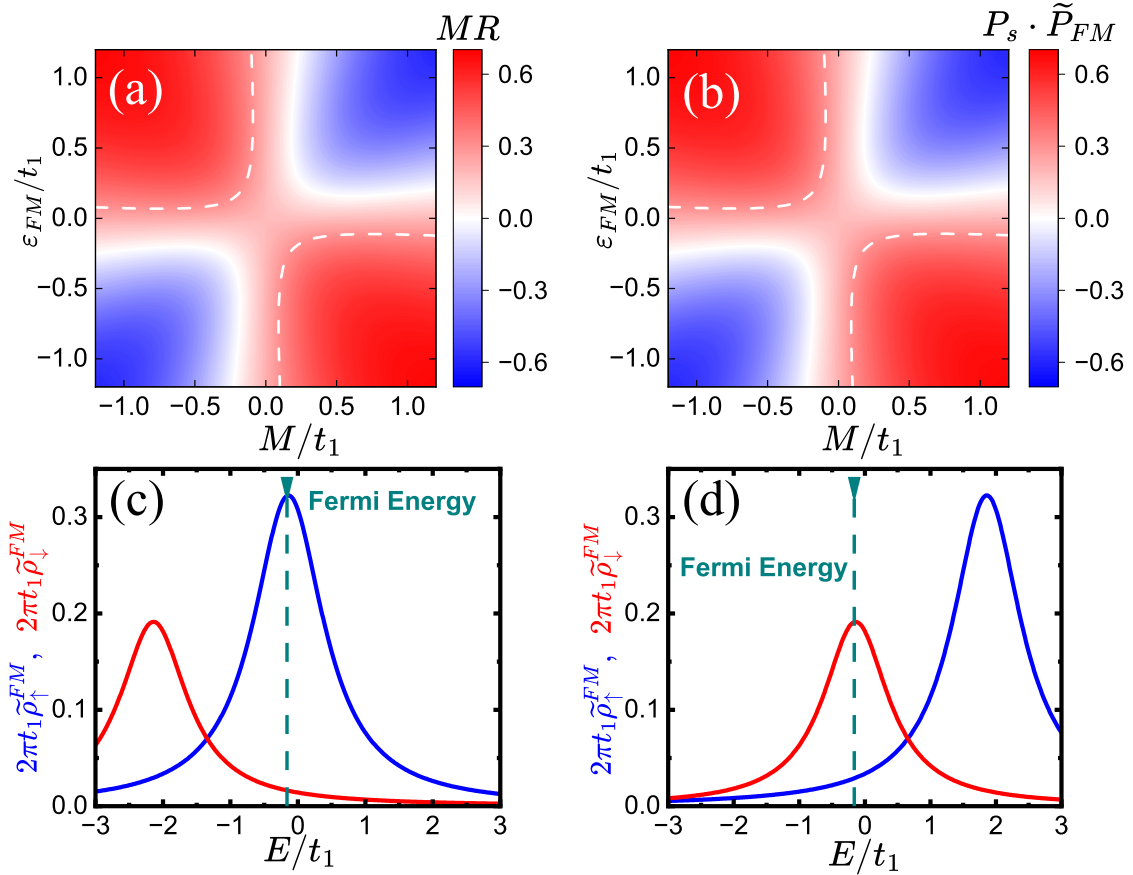


Figure 3: MR vs. parameters of the MPE and the physical mechanism for $MR > P_{FM}$. (a) 2D plot of MR versus the parameters M and ε_{FM} of the MPE at the Fermi level $E = -0.16t_1$. The dashed-white line represents $MR = P_{FM} = 30\%$. (b) $P_s \tilde{P}_{FM}$ as a function of M and ε_{FM} . Here the $P_s \tilde{P}_{FM}$ is almost identical to MR in (a). (c) and (d) Modified spin-up (blue line) and spin-down (red line) DOSs versus the energy E for $M = -\varepsilon_{FM} = t_1$ (c) and $M = \varepsilon_{FM} = t_1$ (d). The green-dashed-vertical lines show $E = -0.16t_1$, the value of which is used in (a,b).

Let us demonstrate analytically why MR can far exceed P_{FM} . The physical mechanism arises from the shift of nonmagnetic-FM interface in the presence of MPE. In the absence of MPE, the nonmagnetic-FM interface locates between the rightmost site, N , of chiral molecules and the FM electrode, as indicated by the red-dashed line in Figure 1a. According to the Jullière model, the device MR always satisfies $MR = P_s P_{FM} < P_{FM}$. While the MPE occurs, the rightmost site is magnetized, and subsequently the nonmagnetic-FM interface is shifted to the position between the $N - 1$ th site and the N th one, see the pink-dashed line Figure 1a. Because of the shift of nonmagnetic-FM interface, the device MR is modified to $MR = P_s \tilde{P}_{FM}$ according to the Jullière model, which depends on the spin polarization \tilde{P}_{FM} of the N th site instead of that in the FM electrode. The modified DOS at the N th site is (see details in Section S1.6 in the Supporting Information):

$$\tilde{\rho}_s^{FM} = \frac{1}{2\pi} \frac{\Gamma_s^{FM}}{(E - \varepsilon_{FM} - sM - \varepsilon_0)^2 + (\Gamma_s^{FM} + \gamma_0)^2 / 4}, \quad (2)$$

where $s = \uparrow (+)$ and $\downarrow (-)$, the linewidth function Γ_s^{FM} is proportional to the DOS ρ_s^{FM} of the FM electrode, and ε_0 , γ_0 are the parameters determined by chiral molecules (see Section S1.6 in the Supporting Information). Consequently, the modified FM polarization is $\tilde{P}_{FM} = (\tilde{\rho}_\uparrow^{FM} - \tilde{\rho}_\downarrow^{FM}) / (\tilde{\rho}_\uparrow^{FM} + \tilde{\rho}_\downarrow^{FM})$ of the N th site, which not only depends on the DOS of the FM electrode but also on the parameters, M and ε_{FM} , of the MPE. For suitable M and ε_{FM} , the modified DOS for specific spin may be very small, resulting in 100% modified polarization \tilde{P}_{FM} so that \tilde{P}_{FM} will be much larger than P_{FM} . As a result, the device $MR = P_s \tilde{P}_{FM}$, can be greater than P_{FM} for large \tilde{P}_{FM} .

Figure 3b shows the analytical result of $P_s \tilde{P}_{FM}$ by using the fitted parameters ε_0 , γ_0 (see details in Section S1.6 in the Supporting Information) and Eq.(2). As compared with Figure 3a, one can see from Figure 3b that the analytical result $P_s \tilde{P}_{FM}$ matches the numerical MR perfectly. This indicates that our theoretical model can quantitatively describe the influence of MPE on chiral molecules.

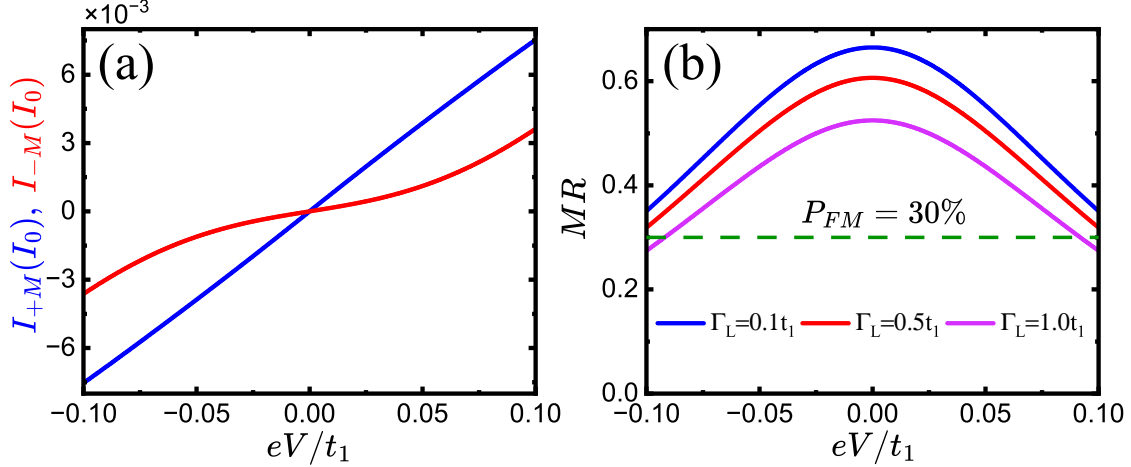


Figure 4: I-V results for finite bias. (a) Current of the device versus the voltage V with the right FM electrode under positive and negative magnetizations for $\Gamma_L = 0.1t_1$. (b) MR versus the voltage V for different Γ_L . The green dashed line is $P_{FM} = 30\%$. In (a) and (b), the SOC strength $s_1 = 0.01t_1$, $E = -0.16t_1$ and $M = -\varepsilon_{FM} = t_1$, and $I_0 = et_1/h$ is the current unit.

To further investigate the influence of MPE, Figure 3c and Figure 3d depict the modified spin-up and spin-down DOSs, $\tilde{\rho}_\uparrow^{FM}$ and $\tilde{\rho}_\downarrow^{FM}$, of the rightmost site N of chiral molecules for $M = -\varepsilon_{FM} = t_1$ and $M = \varepsilon_{FM} = t_1$, respectively. One can see that $\tilde{\rho}_\uparrow^{FM}$ and $\tilde{\rho}_\downarrow^{FM}$ exhibit significant differences in a wide energy range. Specifically, when M and ε_{FM} have opposite sign, according to Eq.(2), $\tilde{\rho}_\uparrow^{FM}$ is much larger than $\tilde{\rho}_\downarrow^{FM}$ at the Fermi energy (see the green-dashed-vertical line in Figure 3c). This large difference leads to greatly modified polarization \tilde{P}_{FM} . When the magnetization parameter is increased, the spin-down DOS $\tilde{\rho}_\downarrow^{FM}$ becomes much smaller and \tilde{P}_{FM} will be very close to 100%. As a result, $MR \approx P_s > P_{FM}$. Contrarily, when M and ε_{FM} have the same sign, $\tilde{\rho}_\downarrow^{FM} > \tilde{\rho}_\uparrow^{FM}$ at the Fermi energy (Figure 3d) and \tilde{P}_{FM} will be reversed, leading to negative MR.

For direct comparison with the experiments, we calculate the current in the N-chiral molecule-FM device under different bias voltages by considering the MPE. The current flowing across the device is given by⁶⁵ $I_{\pm M} = \frac{1}{e} \int_{E-eV/2}^{E+eV/2} G_{\pm M}(\varepsilon) d\varepsilon$, with V the voltage. Then $MR = (I_{+M} - I_{-M})/(I_{+M} + I_{-M})$. In Figure S7a in Supporting Information, we calculate the corresponding I-V curves in the absence of MPE. The difference between I_{+M}

and I_{-M} is too small to generate considerable MR. Figure S7b depicts MR for different electrode-molecule coupling strengths Γ_L . The results show that MR is small, consistently lower than $P_{FM} = 30\%$, exhibits a symmetric shape and a downward shift with increasing Γ_L . The symmetry arises because $I_{\pm M}$ is an odd function of V , making the MR an even function of V . It is worth emphasizing that in the absence of MPE, MR is always lower than P_{FM} , no matter how we change the model parameters, including the SOC strength, the dephasing strength, the electrode-molecule coupling, and the molecular parameters.

The situation completely changes when we consider the MPE. Figure 4a illustrates the currents I_{+M} and I_{-M} versus the voltage V in the presence of MPE. By increasing V , the I-V curves are nonlinear and exhibit antisymmetric behavior. Notably, the difference between I_{+M} and I_{-M} is significantly large over a wide range of voltage, leading to very large MR. Figure 4b shows MR versus the voltage V , which exhibits a symmetric shape and a downward shift with increasing Γ_L . The symmetry arises because $I_{\pm M}$ is an odd function of V , rendering the MR an even function of V . The downward shift can be attributed to the decrease in \tilde{P}_{FM} with increasing Γ_L , as illustrated in Figure S8. It is evident that MR can be much greater than P_{FM} , which is in excellent agreement with the experiments^{36,37,42,59} and violates the Jullière model. The maximum of MR exceeds 60%, which is twice as much as P_{FM} . Furthermore, $MR > P_{FM}$ can occur in a wide range of parameters, although the SOC is extremely weak.

Finally, in the absence of SOC, $s_1 = 0$, the MR is exactly zero (see Figure S9 in the Supporting Information), and the CISS disappears, no matter how we change the structural parameters or whether the MPE is considered. This means that the extremely weak SOC plays a pivotal role for the CISS and the MPE is the determining factor for $MR > P_{FM}$. Also, $MR > P_{FM}$ remains even in the presence of significant twist angle disorder as long as the MPE is included (see Figure S10 in the Supporting Information). Conductance dependence on FM magnetization direction is investigated (see Figure S11 in the Supporting Information). Furthermore, we investigate the double-stranded DNA with the MPE, and

show $MR > P_{FM}$ at the extremely weak SOC (see Section S2, Figure S12 and Figure S13 in the Supporting Information), which validates the robustness and general applicability of our theoretical framework.

In conclusion, the observation of MR beyond the Jullière model for spin selectivity in chiral molecules has puzzled the community for one decade, and here we propose a solution to this problem by taking into account the MPE. Due to the MPE, the nonmagnetic-FM interface is shifted, leading to significant modification of the FM polarization and the device MR far beyond the polarization of the FM electrode. Using a standard numerical approach, we show that the MR indeed exceeds the FM polarization in a wide range of model parameters, even for extremely weak SOC. These results are in good agreement with experimental observations and are expected to end the dispute on the issue of the origin of the CISS. Ultimately, we also hope that the aforementioned results can be verified using first-principles calculations in the future.^{66,67}

ASSOCIATED CONTENT

Supporting Information

The Supporting Information is available free of charge at: https://github.com/btc-99/Supplemental_Information_of_Julliere_Model.

Section S1: The Model of α -helical Protein; Section S2: The spin polarization and MR of Double-Stranded DNA. (PDF)

AUTHOR INFORMATION

Corresponding Author

Qing-Feng Sun – International Center for Quantum Materials, School of Physics, Peking University, Beijing, 100871, China; Hefei National Laboratory, Hefei 230088, China. Email: sunqf@pku.edu.cn

Authors

Tian-Yi Zhang – International Center for Quantum Materials, School of Physics, Peking

University, Beijing, 100871, China

Yue Mao – International Center for Quantum Materials, School of Physics, Peking University, Beijing, 100871, China

Peng-Yi Liu – International Center for Quantum Materials, School of Physics, Peking University, Beijing, 100871, China

Ai-Min Guo – Hunan Key Laboratory for Super-microstructure and Ultrafast Process, School of Physics, Central South University, Changsha 410083, China

Author Contributions

Q.-F.S. designed research; Q.-F.S. supervised the research; T.-Y.Z. performed research; T.-Y.Z. analyzed data; and T.-Y.Z., Y.M., P.-Y.L., A.-M.G., and Q.-F.S. wrote the paper together.

Notes

The authors declare no competing financial interest.

Acknowledgement

This work was financially supported by the National Key R and D Program of China (Grant No. 2024YFA1409002), National Natural Science Foundation of China (Grant No. 12374034, No. 11921005, and No. 12274466), Quantum Science and Technology-National Science and Technology Major Project (2021ZD0302403), and Hunan Provincial Science Fund for Distinguished Young Scholars (Grant No. 2023JJ10058). We also acknowledge the High-performance Computing Platform of Peking University for providing computational resources.

References

- (1) Hsieh, D.; Xia, Y.; Wray, L.; Qian, D.; Pal, A.; others Observation of unconventional quantum spin textures in topological insulators. *Science* **2009**, *323*, 919.

- (2) Bornscheuer, U. T.; Huisman, G. W.; Kazlauskas, R. J.; Lutz, S.; Moore, J. C.; Robins, K. Engineering the third wave of biocatalysis. *Nature* **2012**, *485*, 185.
- (3) Göhler, B.; Hamelbeck, V.; Markus, T. Z.; Kettner, M.; Hanne, G. F.; Vager, Z.; Naaman, R.; Zacharias, H. Spin selectivity in electron transmission through self-assembled monolayers of double-stranded DNA. *Science* **2011**, *331*, 894.
- (4) Alam, K. M.; Pramanik, S. Spin filtering through single-wall carbon nanotubes functionalized with single-stranded DNA. *Adv. Funct. Mater.* **2015**, *25*, 3210.
- (5) Naaman, R.; Paltiel, Y.; Waldeck, D. H. Chiral molecules and the electron spin. *Nat. Rev. Chem.* **2019**, *3*, 250.
- (6) Naaman, R.; Paltiel, Y.; Waldeck, D. H. Chiral molecules and the spin selectivity effect. *J. Phys. Chem. Lett.* **2020**, *11*, 3660.
- (7) Naaman, R.; Waldeck, D. H. Spintronics and chirality: spin selectivity in electron transport through chiral molecules. *Annu. Rev. Phys. Chem.* **2015**, *66*, 263.
- (8) Ray, K.; Ananthavel, S. P.; Waldeck, D. H.; Naaman, R. Asymmetric scattering of polarized electrons by organized organic films of chiral molecules. *Science* **1999**, *283*, 814.
- (9) Xu, Y.; Mi, W. Chiral-induced spin selectivity in biomolecules, hybrid organic–inorganic perovskites and inorganic materials: a comprehensive review on recent progress. *Mater. Horiz.* **2023**, *10*, 1924.
- (10) Sun, R.; Park, K. S.; Comstock, A. H.; McConnell, A.; others Inverse chirality-induced spin selectivity effect in chiral assemblies of π -conjugated polymers. *Nat. Mater.* **2024**, *23*, 782.
- (11) Moharana, A.; Kapon, Y.; Kammerbauer, F.; Anthofer, D.; Yochelis, S.; Shema, H.;

- Gross, E.; Kläui, M.; Paltiel, Y.; Wittmann, A. Chiral-induced unidirectional spin-to-charge conversion. *Sci. Adv.* **2025**, *11*, 1.
- (12) Xie, Z.; Markus, T. Z.; Cohen, S. R.; Vager, Z.; Gutierrez, R.; Naaman, R. Spin specific electron conduction through DNA oligomers. *Nano Lett.* **2011**, *11*, 4652.
- (13) Mishra, D.; Markus, T. Z.; Naaman, R.; Kettner, M.; Göhler, B.; Zacharias, H.; Friedman, N.; Sheves, M.; Fontanesi, C. Spin-dependent electron transmission through bacteriorhodopsin embedded in purple membrane. *Proc. Natl. Acad. Sci. U.S.A.* **2013**, *110*, 14872.
- (14) Kim, Y.-H.; others Chiral-induced spin selectivity enables a room-temperature spin light-emitting diode. *Science* **2021**, *371*, 1129.
- (15) Guo, A.-M.; Sun, Q.-F. Spin-selective transport of electrons in DNA double helix. *Phys. Rev. Lett.* **2012**, *108*, 218102.
- (16) Guo, A.-M.; Sun, Q.-F. Spin-dependent electron transport in protein-like single-helical molecules. *Proc. Natl. Acad. Sci. U.S.A.* **2014**, *111*, 11658.
- (17) Pan, T.-R.; Guo, A.-M.; Sun, Q.-F. Effect of gate voltage on spin transport along α -helical protein. *Phys. Rev. B* **2015**, *92*, 115418.
- (18) Wang, C.; Liang, Z.-R.; Chen, X.-F.; Guo, A.-M.; Ji, G.; Sun, Q.-F.; Yan, Y. Transverse spin selectivity in helical nanofibers prepared without any chiral molecule. *Phys. Rev. Lett.* **2024**, *133*, 108001.
- (19) Zhang, T.-Y.; Mao, Y.; Guo, A.-M.; Sun, Q.-F. Dynamical theory of chiral-induced spin selectivity in electron donor–chiral molecule–acceptor systems. *Phys. Rev. B* **2025**, *111*, 205417.
- (20) Liu, P.-Y.; Zhang, T.-Y.; Sun, Q.-F. Dynamical simulation of chiral-induced spin-polarization and magnetization. *J. Phys. Chem. Lett.* **2025**, *16*, 6500.

- (21) Alwan, S.; Dubi, Y. Spinterface origin for the chirality-induced spin-selectivity effect. *J. Am. Chem. Soc.* **2021**, *143*, 14235.
- (22) Nürenberg, D.; Zacharias, H. Evaluation of spin-flip scattering in chirality-induced spin selectivity using the Riccati equation. *Phys. Chem. Chem. Phys.* **2019**, *21*, 3761.
- (23) Das, T. K.; Tassinari, F.; Naaman, R.; Fransson, J. Temperature-dependent chiral-induced spin selectivity effect: experiments and theory. *J. Phys. Chem. C* **2022**, *126*, 3257.
- (24) Huisman, K. H.; Heinisch, J.-B. M.-Y.; Thijssen, J. M. Chirality-induced spin selectivity (CISS) effect: magnetocurrent–voltage characteristics with coulomb interactions i. *J. Phys. Chem. C* **2023**, *127*, 6900.
- (25) Fransson, J. The chiral induced spin selectivity effect what it is, what it is not, and why it matters. *Isr. J. Chem.* **2022**, *62*, e202200046.
- (26) Kapon, Y.; Zhu, Q.; Yochelis, S.; Naaman, R.; Gutierrez, R.; Cuniberti, G.; Paltiel, Y.; Mujica, V. Probing chiral discrimination in biological systems using atomic force microscopy: The role of van der Waals and exchange interactions. *J. Chem. Phys.* **2023**, *159* (22), 224702.
- (27) Eckvahl, H. J.; Tcyrulnikov, N. A.; Chiesa, A.; Bradley, J. M.; Young, R. M.; Carretta, S.; Krzyaniak, M. D.; Wasielewski, M. R. Direct observation of chirality-induced spin selectivity in electron donor–acceptor molecules. *Science* **2023**, *382*, 197.
- (28) Eckvahl, H. J.; Copley, G.; Young, R. M.; Krzyaniak, M. D.; Wasielewski, M. R. Detecting chirality-induced spin selectivity in randomly oriented radical pairs photogenerated by hole transfer. *J. Am. Chem. Soc.* **2024**, *146*, 24125.
- (29) Latawiec, E. I.; Chiesa, A.; Qiu, Y.; Tcyrulnikov, N. A.; Young, R. M.; Carretta, S.; Krzyaniak, M. D.; Wasielewski, M. R. Detecting chirality-induced spin selectivity in

- chromophore-linked DNA hairpins using photogenerated radical pairs. *Proc. Natl. Acad. Sci. U.S.A.* **2025**, *122*, e2515120122.
- (30) Mondal, P. C.; KantorUriel, N.; Mathew, S. P.; Tassinari, F.; Fontanesi, C.; Naaman, R. Chiral conductive polymers as spin filters. *Adv. Mater.* **2015**, *27*, 1924.
- (31) Abendroth, J. M.; Nakatsuka, N.; Ye, M.; Kim, D.; Fullerton, E. E.; Andrews, A. M.; Weiss, P. S. Analyzing spin selectivity in DNA-mediated charge transfer via fluorescence microscopy. *ACS Nano* **2017**, *11*, 7516.
- (32) Aizawa, H.; Sato, T.; Maki-Yonekura, S.; Yonekura, K.; Takaba, K.; Hamaguchi, T.; Minato, T.; Yamamoto, H. M. Enantioselectivity of discretized helical supramolecule consisting of achiral cobalt phthalocyanines via chiral-induced spin selectivity effect. *Nat. Commun.* **2023**, *14*, 4530.
- (33) Adhikari, Y.; Liu, T.; Wang, H.; Hua, Z.; Liu, H.; Lochner, E.; Schlottmann, P.; Yan, B.; Zhao, J.; Xiong, P. Interplay of structural chirality, electron spin and topological orbital in chiral molecular spin valves. *Nat. Commun.* **2023**, *14*, 5163.
- (34) Kiran, V.; Cohen, S. R.; Naaman, R. Structure dependent spin selectivity in electron transport through oligopeptides. *J. Chem. Phys.* **2017**, *146* (9), 092302.
- (35) Liu, T.; others Linear and nonlinear two-terminal spin-valve effect from chirality-induced spin selectivity. *ACS Nano* **2020**, *14*, 15983.
- (36) Mishra, S.; Pirbadian, S.; Mondal, A. K.; El-Naggar, M. Y.; Naaman, R. Spin-dependent electron transport through bacterial cell surface multiheme electron conduits. *J. Am. Chem. Soc.* **2019**, *141*, 19198.
- (37) Kulkarni, C.; Mondal, A. K.; Das, T. K.; Grinbom, G.; Tassinari, F.; Mabesoone, M. F. J.; Meijer, E. W.; Naaman, R. Highly efficient and tunable filtering of electrons'

- spin by supramolecular chirality of nanofiber-based materials. *Adv. Mater.* **2020**, *32*, 1904965.
- (38) Tedrow, P. M.; Meservey, R. Spin-dependent tunneling into ferromagnetic nickel. *Phys. Rev. Lett.* **1971**, *26*, 192.
- (39) Julliere, M. Tunneling between ferromagnetic films. *Phys. Lett. A* **1975**, *54*, 225.
- (40) Moodera, J. S.; Mathon, G. Spin polarized tunneling in ferromagnetic junctions. *J. Magn. Magn. Mater.* **1999**, *200*, 248.
- (41) Huizi-Rayo, U.; Gutierrez, J.; Seco, J. M.; Mujica, V.; Diez-Perez, I.; Ugalde, J. M.; Tercjak, A.; Cepeda, J.; Sebastian, E. S. An ideal spin filter: long-range, high-spin selectivity in chiral helicoidal 3-dimensional metal organic frameworks. *Nano Lett.* **2020**, *20*, 8476.
- (42) Lu, H.; others Highly distorted chiral two-dimensional tin iodide perovskites for spin polarized charge transport. *J. Am. Chem. Soc.* **2020**, *142*, 13030.
- (43) Al-Bustami, H.; Khaldi, S.; Shoseyov, O.; Yochelis, S.; Killi, K.; Berg, I.; Gross, E.; Paltiel, Y.; Yerushalmi, R. Atomic and molecular layer deposition of chiral thin films showing up to 99% spin selective transport. *Nano Lett.* **2022**, *22*, 5022.
- (44) Mishra, S.; Mondal, A. K.; Pal, S.; Das, T. K.; Smolinsky, E. Z. B.; Siligardi, G.; Naaman, R. Length-dependent electron spin polarization in oligopeptides and DNA. *J. Phys. Chem. C* **2020**, *124*, 10776.
- (45) Waldeck, D. H.; Naaman, R.; Paltiel, Y. The spin selectivity effect in chiral materials. *APL Mater.* **2021**, *9*, 040902.
- (46) Alwan, S.; Sharoni, A.; Dubi, Y. Role of electrode polarization in the electron transport chirality-induced spin-selectivity effect. *J. Phys. Chem. C* **2024**, *128*, 6438.

- (47) Liu, T.; Weiss, P. S. Spin polarization in transport studies of chirality-induced spin selectivity. *ACS Nano* **2023**, *17*, 19502.
- (48) Pan, T.-R.; Guo, A.-M.; Sun, Q.-F. Spin-polarized electron transport through helicene molecular junctions. *Phys. Rev. B* **2016**, *94*, 235448.
- (49) Sun, Q.-F.; Xie, X. C. Spontaneous spin-polarized current in a nonuniform Rashba interaction system. *Phys. Rev. B* **2005**, *71*, 155321.
- (50) Sun, Q.-F.; Wang, J.; Guo, H. Quantum transport theory for nanostructures with Rashba spin-orbital interaction. *Phys. Rev. B* **2005**, *71*, 165310.
- (51) Liu, P.-Y.; Zhang, T.-Y.; Guo, A.-M.; Paltiel, Y.; Sun, Q.-F. Spin-to-charge conversion modulated by chiral molecules. *J. Phys. Chem. Lett.* **2025**, *16*, 10426.
- (52) Zhang, T.-Y.; Liu, P.-Y.; Guo, A.-M.; Sun, Q.-F. Spin-to-charge conversion driven by inverse chiral-induced spin selectivity. *arXiv preprint arXiv:2509.04022* **2025**, Submission date: 2025-09-04, URL: <https://arxiv.org/abs/2509.04022> (Accessed: 2025-10-27).
- (53) Yan, Y. J.; Zhang, H. Toward the mechanism of long-range charge transfer in DNA: Reduced density matrix approach. *J. Theor. Comput. Chem.* **2002**, *01*, 225.
- (54) Steele, G. A.; Pei, F.; Laird, E. A.; Jol, J. M.; Meerwaldt, H. B.; Kouwenhoven, L. P. Large spin-orbit coupling in carbon nanotubes. *Nat. Commun.* **2013**, *4*, 1573.
- (55) Xing, Y.; Sun, Q.-F.; Wang, J. Symmetry and transport property of spin current induced spin-Hall effect. *Phys. Rev. B* **2007**, *75*, 075324.
- (56) Schwöbel, J.; Fu, J. B.; Dilullo, G. H.; Klyatskaya, S.; Ruben, M.; Wiesendanger, R. Real-space observation of spin-split molecular orbitals of adsorbed single-molecule magnets. *Nat. Commun.* **2012**, *3*, 953.

- (57) Kawahara, S. L.; Lagoute, J.; Repain, V.; C. Chacon, Y. G.; Rousset, S.; Smogunov, A.; Barreteau, C. Large magnetoresistance through a single molecule due to a spin-split hybridized orbital. *Nano Lett.* **2012**, *12*, 4558.
- (58) Perrin, M. L.; Verzijl, C. J. O.; Martin, C. A.; Shaikh, A. J.; Eelkema, R.; Esch, J. H. V.; Ruitenbeek, J. M. V.; Thijssen, J. M.; Zant, H. S. J. V. D.; Dulić, D. Large tunable image-charge effects in single-molecule junctions. *Nature Nanotech.* **2013**, *8*, 282.
- (59) Lu, H.; Wang, J.; Xiao, C.; Pan, X.; Chen, X.; Brunecky, R.; Berry, J. J.; Zhu, K.; Beard, M. C.; Vardeny, Z. V. Spin-dependent charge transport through 2D chiral hybrid lead-iodide perovskites. *Sci. Adv.* **2019**, *5*, eaay0571.
- (60) Xing, Y.; Sun, Q. F.; Wang, J. Influence of dephasing on the quantum Hall effect and the spin Hall effect. *Phys. Rev. B* **2008**, *77*, 115346.
- (61) Jiang, H.; Cheng, S.; Sun, Q. F.; Xie, X. C. Topological insulator: a new quantized spin Hall resistance robust to dephasing. *Phys. Rev. Lett.* **2009**, *103*, 036803.
- (62) Morita, T.; Kimura, S. Long-range electron transfer over 4 nm governed by an inelastic hopping mechanism in self-assembled monolayers of helical peptides. *J. Am. Chem. Soc.* **2003**, *125*, 8732.
- (63) Skourtis, S. S.; Balabin, I. A.; Kawatsu, T.; Beratan, D. N. Protein dynamics and electron transfer: Electronic decoherence and non-Condon effects. *Proc. Natl. Acad. Sci. U.S.A.* **2005**, *102*, 3552.
- (64) Cordes, M.; Giese, B. Electron transfer in peptides and proteins. *Chem. Soc. Rev.* **2009**, *38*, 892.
- (65) Datta, S. *Electronic Transport in Mesoscopic Systems*, 1st ed.; Cambridge University Press, 1995.

- (66) Wang, J.; Yang, X.; Yang, Z.; Lu, J.; Ho, P.; Wang, W.; Ang, Y. S.; Cheng, Z.; Fang, S. Pentagonal 2D altermagnets: Material screening and altermagnetic tunneling junction device application. *Adv. Funct. Materials* **2025**, *202505145*.
- (67) Yang, Z.; Yang, X.; Wang, J.; Li, Q.; Peng, R.; Lee, C. H.; Ang, L. K.; Lu, J.; Ang, Y. S.; Fang, S. Unconventional tunnel magnetoresistance scaling with altermagnets. *arXiv preprint arXiv:2505.17192* **2025**, Submission date: 2025-05-22, URL: <https://arxiv.org/abs/2505.17192> (Accessed: 2025-10-27).

TOC Graphic

